Received 18 October 2021; revised 17 November 2021; accepted 30 November 2021. Date of publication 9 December 2021; date of current version 22 December 2021.

Digital Object Identifier 10.1109/OJCOMS.2021.3134091

Enhancing the Reliability of Dense LoRaWAN Networks With Multi-User Receivers

JOACHIM TAPPAREL [1], MATHIEU XHONNEUX [2] (Graduate Student Member, IEEE), DAVID BOL [2] (Senior Member, IEEE), JÉRÔME LOUVEAUX [2] (Member, IEEE), AND ANDREAS BURG [1] (Senior Member, IEEE)

[1] Telecommunication Circuits Laboratory, École Polytechnique Fédérale de Lausanne, 1015 Lausanne, Switzerland
[2] Institute of Information and Communication Technologies, Electronics and Applied Mathematics, Université catholique de Louvain, 1348 Louvain-la-Neuve, Belgium

CORRESPONDING AUTHOR: J. TAPPAREL (e-mail: joachim.tapparel@epfl.ch)

ABSTRACT LoRaWAN is a low-power wireless technology that provides long-range connectivity to battery-powered Internet of Things (IoT) devices. To minimize the energy consumption of the IoT nodes, LoRaWAN networks use for the uplink a pure non-slotted ALOHA multiple access scheme. Since the devices are not synchronized in time, collisions between uplink packets are the main source of errors when the number of nodes becomes important. To improve the reliability of dense LoRaWAN networks, we propose in this paper a successive interference cancellation LoRa receiver capable of decoding frames from two colliding users. The proposed two-user detector leverages the bit-interleaved coded modulation scheme of LoRa to improve the detection and cancellation of the strongest interfering user. We show that in the presence of two interfering users, the usage of a low coding-rate and iterative soft-detection are essential to attain error rates sufficiently close to the single-user scenario. Using network-level simulations, we subsequently evaluate the gains of our proposed two-user receiver in a realistic LoRaWAN network. To this end, we build advanced models of the studied receivers using Monte-Carlo simulations at the physical layer. For an overall packet error rate of 1%, simulation results indicate that a LoRaWAN network employing our two-user detector may serve 4.7 times more devices than a network with only a single-user receiver at the gateway.

INDEX TERMS ALOHA, bit-interleaved coded modulation (BICM), Internet of Things (IoT), iterative soft-demodulation, LoRa, multi-user receiver, network simulation, successive interference cancellation (SIC).

I. INTRODUCTION

IN THE past decade, LoRaWAN has emerged as the most popular wireless technology for ultra low-power Internet of Things (IoT) devices. To achieve long range communications in a stringent energy budget, its physical (PHY) layer, simply named LoRa, uses a chirp spread spectrum (CSS) modulation combined with Hamming codes in a bit-interleaved coded modulation (BICM) scheme [1], [2]. The spreading gain of the CSS modulation is determined by the spreading factor (SF), which allows to trade off data rate and energy for coverage [3].

Despite its wide adoption, it is well-known that LoRaWAN suffers from scalability limitations [4], [5]. To avoid an energy-intensive synchronization mechanism between IoT devices, LoRaWAN uses a pure (non-slotted) ALOHA multiple access scheme. Since devices sharing the same SF employ the same waveforms, collisions between users may occur and even cause the network throughput to rapidly decrease for an increasing number of users [6], [7]. On the other hand, the demodulation of LoRa symbols is inherently resistant against interference from packets using different spreading factors. A LoRa receiver benefits on average from a co-channel rejection of -16 dB for inter-SF interference [8].

Experimental studies have shown that for concurrent same-SF transmissions of two users, the strongest user is usually correctly decoded provided a sufficiently large signal-to-interference ratio (SIR), between 1 dB and 3 dB depending

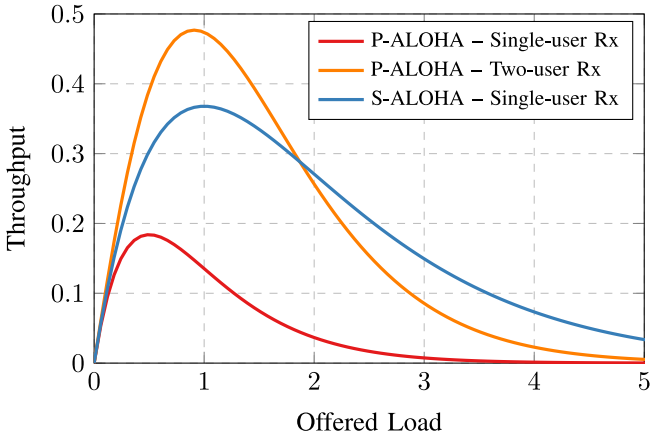

FIGURE 1. Throughput of pure ALOHA (P-ALOHA) and slotted ALOHA (S-ALOHA) networks. In this work, we design a two-user LoRa receiver and evaluate its performance in a pure ALOHA network.

on the signal-to-noise ratio (SNR) [8]–[10]. This behavior, usually referred to as the *capture effect*, has been confirmed through analytical results on the PHY layer, but only for the case of uncoded transmissions [11]. The potential benefits of leveraging the coding in the BICM scheme against same-SF interference, and the corresponding improvements of the network throughput, have not been investigated so far.

As of today, two main approaches have been followed in the literature to overcome same-SF collisions, which are the dominating error events in interference-limited LoRaWAN networks. Below, we briefly summarize these attempts, and we further explain why multi-user LoRa receivers are a promising, but also challenging, solution to improve the reliability and scalability of LoRaWAN networks.

A. APPROACHES TO IMPROVE LORAWAN AT THE MAC LAYER

Several improvements at the MAC layer have been proposed over the last years to overcome the same-SF interference issue. These solutions either extend the underlying ALOHA multiple access of LoRaWAN [12]–[16] or design new MAC layer synchronization mechanisms [17]–[19].

In the first category, carrier sense multiple access (CSMA) has been investigated in [12]–[14], with LoRa devices implementing a listening before talk (LBT) mechanism. Although CSMA helps to prevent collisions for users close to the gateway, it offers little gain over pure ALOHA in realistic networks because of the hidden terminal problem [13]. In [15], [16], a time synchronization algorithm is designed and implemented on top of the traditional LoRaWAN specifications. For each SF, the channel is divided into time slots and the transmissions of the devices are regulated to fit into these slots, which allows the network to benefit from the throughput increase of slotted ALOHA, as shown in Fig. 1.

To completely avoid the issue of collisions, other works in the literature seek to implement time-division multiple access (TDMA). In such schemes, the gateways periodically send beacons that enable the devices to obtain an accurate time reference for their transmissions. In [17], a static distribution of the time slots based on the addresses of the devices is performed when they connect to the network. In [18], the gateway performs a fine-grained scheduling of the time slots and regularly broadcasts the time-resource repartition to all devices. These TDMA schemes however oblige the end nodes to listen to beacons from the gateway to maintain their synchronization in time, which greatly increases their power consumption.

B. MULTI-USER RECEIVERS FOR DENSE LORAWAN NETWORKS

In this paper, we aim to improve the reliability and scalability of LoRaWAN networks without negatively impacting the energy consumption of the nodes, i.e., by keeping pure ALOHA as multiple access scheme. Instead of modifying the MAC layer, we propose a two-user LoRa receiver capable of demodulating two colliding users with the same SF. This receiver is located at the mains-powered gateway, which does not suffer from energy constraints. To anticipate the possible gains of such a receiver, the theoretical throughput of a pure ALOHA network with an ideal two-user receiver is shown in Fig. 1 [20], [21]. At the optimal offered load, the deployment of a two-user receiver can triple the network throughput compared to a conventional single-user receiver, and can even surpass the performance of slotted ALOHA without requiring any time synchronization between the devices. In a similar spirit, but by means of stochastic geometry, the authors of [22] evaluate that the usage of a two-user SIC receiver allows to increase the number of nodes in a network by 2.59, without deteriorating its reliability.

Yet, the design of an efficient two-user receiver has only recently received the appropriate attention. Several initial LoRa multi-user receivers have so far been proposed [23]–[29]. The receivers presented in [23]–[26] demodulate all the symbols received during a single symbol period, and subsequently try to attribute the demodulated signals to their corresponding user. In [23], the different frequency offsets between the users are used to distinguish their symbols. In [24], the received power of each user is also leveraged for the decision, whereas in [25], both the time and frequency offsets between users are used. The authors of [26] propose a scaled despreading operation that allows a more robust estimation of the time offset between the colliding users and hence of their corresponding symbols. These receivers, however, all rely on a joint demodulation of the colliding symbols, which is difficult to perform at the low SNR levels (-25 dB to -5 dB) at which LoRa commonly operates.

On the contrary, the receivers of [27]–[29] implement interference cancellation mechanisms that enable separate detections of the colliding symbols. A parallel interference cancellation LoRa receiver relying on the differences in carrier frequencies and received powers between users is introduced in [27]. Similarly, two successive interference cancellation (SIC) receivers are presented in [28] and [29]. Most notably, the authors of [28] show that their SIC receiver is capable of efficiently demodulating the user with the

strongest received power, but the bit error rates of the weaker users all floor between 10^{-4} and 10^{-3}. None of these receivers explicitly takes advantage of the BICM scheme in conjunction with soft decoding and all fail to exhibit useful error rates at realistic SNRs. As a consequence, the evaluation of the performance of a practical LoRaWAN network with an efficient, but realistic, model of a two-user gateway is also missing in the literature.

Contributions: In this work, we improve our successive interference cancellation (SIC) LoRa two-user detector capable of demodulating two colliding users with the same SF, which has initially been introduced in [30]. This detector explicitly leverages the BICM scheme of the LoRa PHY by performing both a soft-demodulation and soft-decoding of the colliding users. We show that leveraging the coding is essential to attain useful error rates in the target SNR regime. Further, we evaluate the benefits of deploying our proposed two-user detector in a LoRaWAN network. The network simulation results, obtained by extending the LoRaWAN module [7] of the ns-3 simulator, indicate that for a target packet error rate of 1%, our proposed detector is capable of serving 4.7 times more LoRa end nodes than a conventional single-user gateway.

Outline: The remainder of this paper is organized as follows. In Section II, we provide a brief description of the LoRa physical layer. We also explain the implementation of a single-user LoRa soft-receiver, and eventually describe the signal model of two interfering LoRa users sharing the same SF. In Section III, we design an iterative two-user SIC soft-detector and evaluate its performance for different parameters (coding rate, spreading factor, ...). Finally, we evaluate and discuss in Section IV the impact of our proposed receiver on the scalability and reliability of a LoRaWAN network.

II. THE LORA PHYSICAL LAYER

In this section, we provide a brief explanation of the LoRa physical layer. We first introduce how LoRa implements BICM with its particular chirp spread spectrum modulation and we subsequently explain how a conventional single-user LoRa receiver performs soft-demodulation and soft-decoding of the received symbols. In preparation for the next section, we then extend the single-user signal model to include two interfering LoRa users employing the same spreading factor.

A. THE LORA TX CHAIN

To enable energy-efficient long range communications, LoRa uses a spread spectrum modulation with $N = 2^{\mathrm{SF}}$ orthogonal waveforms [31], where $\mathrm{SF} \in \{7, \ldots, 12\}$ is called the *spreading factor*. The waveforms are chirps, i.e., complex phasors whose instantaneous frequency increases linearly over time and spans a bandwidth $B \in \{125, 250, 500\}$ kHz. Each waveform consists of N samples when sampled at the frequency $f_S = B$ and encodes SF bits of information. Increasing the spreading factor SF increases the spreading gain of the modulation, and thus the communication range, but at the expense of decreasing the data rate. A symbol $s \in \{0, \ldots, N-1\}$

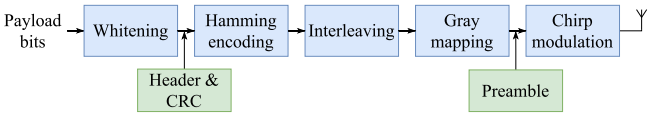

FIGURE 2. Illustration of the LoRa PHY Tx chain, which implements Bit-Interleaved Coded Modulation.

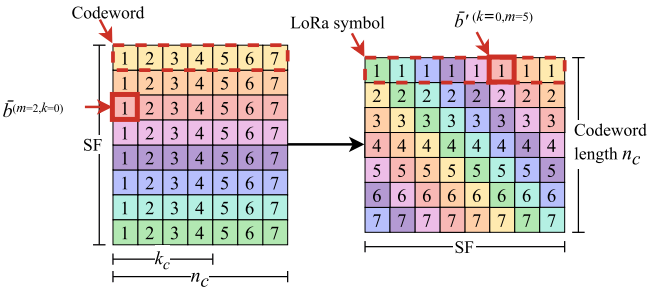

FIGURE 3. LoRa interleaving for SF = 8 and a (4, 7) Hamming code.

is modulated to the discrete-time baseband-equivalent signal $x_s[n]$ by selecting the initial frequency of the chirp [31], [32]

$$x_s[n] = \begin{cases} e^{j2\pi\left(\frac{n^2}{2N}\left(\frac{B}{f_S}\right)^2+\left(\frac{s}{N}-\frac{1}{2}\right)\left(\frac{B}{f_S}\right)n\right)}, & 0 \le n < n_f, \\ e^{j2\pi\left(\frac{n^2}{2N}\left(\frac{B}{f_S}\right)^2+\left(\frac{s}{N}-\frac{3}{2}\right)\left(\frac{B}{f_S}\right)n\right)}, & n_f \le n < N, \end{cases} \quad (1)$$

where $n_f = N - s$ is the sample index at which a frequency step of $-B$ occurs such that the modulated signal remains in the allocated bandwidth.

To improve its robustness against noise, interference, and residual time and frequency offsets, LoRa combines its chirp spread spectrum modulation with an error correcting code using BICM [33]. A LoRa transmitter, illustrated in Fig. 2, consists of the serial concatenation of a Hamming encoder with the N-dimensional memoryless chirp modulation through a bit interleaver and a one-to-one binary Gray labeling [2], [32]. Conventional (k_c, n_c) Hamming codes with $k_c = 4$ and $n_c \in \{5, 6, 7, 8\}$ are used, where k_c denotes the data word length and n_c denotes the codeword length. The interleaving stage is a simple block diagonal interleaver with the arrangement shown in Fig. 3. The Gray labeling then maps groups of SF bits into symbols $s \in \{0, \ldots, N-1\}$.

Beside the previously mentioned blocks, the Tx chain also includes a whitening block, the addition of a header and a cyclic redundancy check (CRC) to the whitened payload bits, and the concatenation of a preamble before the modulated symbols. The whitening is a simple XOR operation with a known pseudo-random sequence and has no effect on the performance. We hence ignore the whitening in the remainder of this paper. The header indicates to the receiver the length of the packet, the code rate $\mathrm{CR} = {}^{k_c}/_{n_c}$ and the presence of a CRC [34].

B. DETECTION AND DECODING FOR LORA

Iterating between a soft-input soft-output (SISO) demodulator and a SISO decoder is an efficient approach to improve

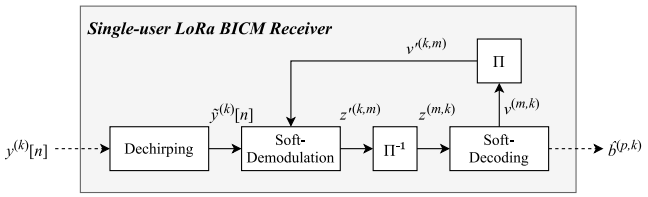

FIGURE 4. Illustration of an iterative BICM LoRa soft-receiver.

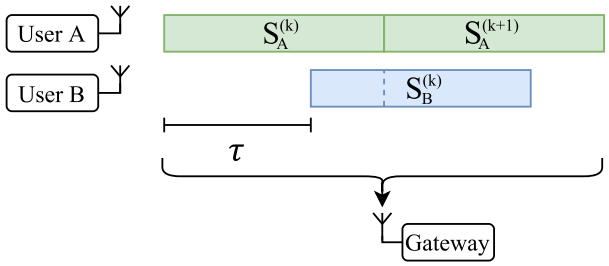

FIGURE 5. Illustration of the asynchronicity in time between the users A and B, with the sampling time offset τ.

the error rate performance over non-iterative receivers [35]. The architecture of such an iterative single-user LoRa receiver [1] is shown in Fig. 4. To describe its functioning, we now consider only one user transmitting a sequence of k_cSF payload bits over an AWGN channel. As annotated in Fig. 3, we denote the transmitted payload bits as $b^{(m,p)}$ with $m \in \{0, \ldots, \mathrm{SF}-1\}$ and $p \in \{0, \ldots, k_c - 1\}$ denoting the row and column, respectively, of the bit matrix before encoding and interleaving. Further, let $\bar{b}^{(m,k)}$ and $\bar{b}'^{(k,m)}$ with $k \in \{0, \ldots, n_c - 1\}$ be the corresponding coded bits before and after interleaving, respectively. The n_c rows of bits $\bar{b}'^{(k,m)}$ are mapped to the symbols $x^{(k)}[n]$ using (1).

The corresponding n_c received LoRa symbols are represented by $y^{(k)}[n] = h^{(k)}x^{(k)}[n] + w^{(k)}[n]$, where $n \in \{0, \ldots, N-1\}$, $w^{(k)}[n] \sim \mathcal{CN}(0, \sigma^2)$ is complex AWGN with variance σ^2 and $h^{(k)} \in \mathbb{C}$ is the complex-valued channel gain during the transmission of the k-th symbol. In this paper, we assume that the magnitudes of the gains $h^{(k)}$ are constant and equal to $\sqrt{P}$ during the whole packet reception, whereas the phase of $h^{(k)}$ may change over time due to limited accuracy of the low-cost crystals embedded in IoT devices [36]. Hence, we define for each symbol a different starting phase $\theta^{(k)} = \angle h^{(k)}$.

LoRa receivers typically perform a non-coherent detection of the received symbols to avoid the tracking of the phase $\theta^{(k)}$ [32], [34]. For this kind of detection, the likelihood that the transmitter sent the candidate symbol $\bar{s}$ during the k-th window is given by [37], [38]

$$\Lambda(\bar{s}|y^{(k)}) = C \cdot I_0\left(\frac{\sqrt{P}}{\sigma^2}\left|\sum_{n=0}^{N-1} y[n] e^{-j2\pi\left(\frac{n^2}{2N} + n\left(\frac{\bar{s}}{N} - \frac{1}{2}\right)\right)}\right|\right), \quad (2)$$

where $I_0(x)$ is the first order modified Bessel function of the first kind and C is a constant common to all symbols. To allow a more intuitive understanding of (2), an intermediate *dechirping* stage is often introduced in the receiver. This stage performs a pointwise multiplication of the received signal with $x_0^*[n]$, the complex conjugate of an unmodulated symbol: $\tilde{y}^{(k)}[n] = y^{(k)}[n] \cdot x_0^*[n] = h^{(k)}\frac{s^{(k)}n}{N} + \tilde{w}^{(k)}[n]$, where $\tilde{w}^{(k)}[n] = w^{(k)}[n] \cdot x_0^*[n]$. The summation in (2) then becomes a discrete Fourier transform (DFT) of the dechirped signal

$$\Lambda(\bar{s}|y^{(k)}) = C \cdot I_0\left(\frac{\sqrt{P}}{\sigma^2}\left|Y^{(k)}[\bar{s}]\right|\right), \quad (3)$$

where $Y^{(k)}[\bar{s}]$ is the N-point DFT of $\tilde{y}^{(k)}[n]$.

To compute soft information at the output of the demodulator, the likelihoods $\Lambda(\bar{s}|y^{(k)})$ are mapped to log-likelihood ratios (LLRs) [35]

$$z'^{(k,m)} = \log \frac{\sum_{\bar{s}:g_m(\bar{s})=1} \Lambda\left(\bar{s}|y^{(k)}\right) \prod_{i=0,i\neq m}^{\mathrm{SF}-1} e^{g_i(\bar{s})v'^{(k,i)}}}{\sum_{\bar{s}:g_m(\bar{s})=0} \Lambda\left(\bar{s}|y^{(k)}\right) \prod_{i=0,i\neq m}^{\mathrm{SF}-1} e^{g_i(\bar{s})v'^{(k,i)}}}, \quad (4)$$

where $g_i(\bar{s})$ returns the i-th bit of the symbol $\bar{s}$ in the Gray labeling, and $v'^{(k,m)}$ are the apriori LLRs computed by the soft Hamming decoder after re-interleaving. During the first iteration, we have $v'^{(k,m)} = 0$. In practical receivers, the complexity of computing the LLRs $z'^{(k,m)}$ is reduced by using the max-log approximation [39], which here yields

$$z'^{(k,m)} = \max_{\bar{s}:g_m(\bar{s})=1}\left[\log I_0\left(\frac{\sqrt{P}}{\sigma^2}|Y[\bar{s}]|\right) + \sum_{i=0,i\neq m}^{\mathrm{SF}-1} g_i(\bar{s})v'^{(k,i)}\right] - \max_{\bar{s}:g_m(\bar{s})=0}\left[\log I_0\left(\frac{\sqrt{P}}{\sigma^2}|Y[\bar{s}]|\right) + \sum_{i=0,i\neq m}^{\mathrm{SF}-1} g_i(\bar{s})v'^{(k,i)}\right]. \quad (5)$$

The LLRs $z'^{(k,m)}$ are subsequently de-interleaved and fed to a Hamming soft-decoder (e.g., [40]). This soft-decoder outputs new LLR values $v^{(m,k)}$, from which an estimation $\hat{b}^{(m,p)}$ of the transmitted bits is obtained. To further improve the receiver performance, several iterations between the soft-demodulator and the soft-detector may occur. To this end, the LLRs $v^{(m,k)}$ are re-interleaved and fed as apriori information $v'^{(k,m)}$ to the soft-demodulator.

C. SIGNAL MODEL FOR TWO INTERFERING USERS

We now extend the model to two superimposed users with the same SF, namely user A and user B. This model has previously been derived in [41] and is the basis for the construction of the iterative two-user detector in Section III. Let us define $s_{\mathrm{A}}^{(k)}$ and $s_{\mathrm{B}}^{(k)}$ as the k-th colliding symbols sent by users A and B, respectively. The symbols $s_{\mathrm{A}}^{(1)}$ and $s_{\mathrm{B}}^{(1)}$ are hence the two first information symbols of both users that collide with each other. Due to the non-slotted ALOHA multiple access scheme, the users are not synchronized to each other in time. We define $\tau \in [0, N)$ as the relative sample-level time offset between the first sample of the first colliding symbol transmitted by user A and the first sample of the first colliding symbol of user B, as illustrated in Fig. 5.

This offset can be split into an integer part $L_{\text{STO}} = \lceil \tau \rceil$ and a non-integer part $\lambda_{\text{STO}} = \tau - \lceil \tau \rceil$ [11]. In order to simplify the notation of the model, we also assume that the gateway is synchronized in both frequency and time to user A.

Since the transmission of user B experiences an STO $\tau \geq 0$ with respect to user A, the first $\lceil \tau \rceil$ samples of symbol $s_{\text{A}}^{(k)}$ overlap with symbol $s_{\text{B}}^{(k-1)}$ and the last $N - \lceil \tau \rceil$ samples of symbol $s_{\text{A}}^{(k)}$ overlap with symbol $s_{\text{B}}^{(k)}$. The contribution of user B to the k-th window of N samples $y^{(k)}[n]$ can therefore be split into two parts, namely $y_{\text{B},1}^{(k)}[n]$ for $n \in \mathcal{N}_1 = \{0, \ldots, \lceil \tau \rceil - 1\}$ and $y_{\text{B},2}^{(k)}[n]$ for $n \in \mathcal{N}_2 = \{\lceil \tau \rceil, \ldots, N-1\}$, with

$$y_{\text{B},1}^{(k)}[n] = e^{j2\pi\left(\frac{(n+N-\tau)^2}{2N} + (n+N-\tau)\left(\frac{s_{\text{B}}^{(k-1)}}{N} - \frac{1}{2} - u\left[n - n_{f,1}^{(k)}\right]\right)\right)},$$

$$y_{\text{B},2}^{(k)}[n] = e^{j2\pi\left(\frac{(n-\tau)^2}{2N} + (n-\tau)\left(\frac{s_{\text{B}}^{(k)}}{N} - \frac{1}{2} - u\left[n - n_{f,2}^{(k)}\right]\right)\right)},$$

and $n_{f,1}^{(k)} = \lceil \tau \rceil - s_{\text{B}}^{(k-1)}$, $n_{f,2}^{(k)} = N + \lceil \tau \rceil - s_{\text{B}}^{(k)}$ [41], [42].

Prior to synchronization, both users are affected by distinct carrier frequency offsets relative to the receiver, namely $\Delta f_{c,\text{A}}$ and $\Delta f_{c,\text{B}}$. However, since we assume that the receiver is synchronized to user A, there is a single residual CFO $\Delta f_c = \Delta f_{c,\text{B}} - \Delta f_{c,\text{A}}$ that only affects the signal from user B. Also, let P_{A} and P_{B} be the received powers of users A and B, respectively. As previously explained, we do not make any assumption on the phase coherence of successive symbols, and thus define $\theta_{\text{A}}^{(k)}$ and $\theta_{\text{B}}^{(k)}$ as the initial independent phases of the corresponding symbols of user A and B, respectively. The baseband-equivalent model of the sampled signal contained in the k-th window of N samples is therefore

$$y^{(k)}[n] = \sqrt{P_{\text{A}}} e^{j\theta_{\text{A}}^{(k)}} x_{s_{\text{A}}^{(k)}}[n] + w^{(k)}[n] + \begin{cases} \sqrt{P_{\text{B}}} e^{j\theta_{\text{B}}^{(k-1)}} c[n] y_{\text{B},1}^{(k)}[n], & n \in \mathcal{N}_1, \\ \sqrt{P_{\text{B}}} e^{j\theta_{\text{B}}^{(k)}} c[n] y_{\text{B},2}^{(k)}[n], & n \in \mathcal{N}_2, \end{cases} \quad (6)$$

where $c[n] = e^{j2\pi n \frac{\Delta f_c}{f_s}}$ is the residual CFO affecting user B.

III. A TWO-USER SUCCESSIVE INTERFERENCE CANCELLATION LORA SOFT-DETECTOR

Motivated by the resilience of the BICM scheme against time-varying channels, we present in this section a two-user SIC soft-detector derived from the previously described iterative single-user detector. This detector demodulates simultaneously two interfering users that overlap in time with the same SF. The strongest user is first decoded and its contribution to the received signal is removed from the received signal before the weakest user is decoded. Since LoRa uses an orthogonal symbol alphabet, the usage of conventional soft-interference cancellation schemes is not straightforward. Our proposed two-user detector performs instead a hard interference cancellation of the strongest user, while still leveraging the soft-output of the Hamming decoding.

In a practical gateway, an instance of this detector should be deployed for each SF, since users with different SFs can be demodulated in parallel without interfering significantly with each other. Since we have already demonstrated in a previous paper that two-user synchronization can easily be achieved [41], we assume for the remainder of this paper that the proposed two-user detector is always synchronized to the strongest user and that it has perfect knowledge of the users received powers P_{A} and P_{B}, and of the STO τ and the residual CFO Δf_c between them.

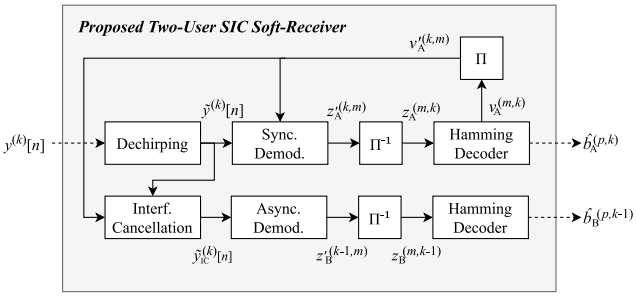

FIGURE 6. Illustration of the proposed two-user SIC soft-receiver.

The architecture of the proposed detector is described first. We then explain in detail its interference-cancellation algorithm and the asynchronous soft-demodulator used to detect the symbols of the non-synchronized weak user. An analysis of the performance of the two-user detector concludes this section.

A. ARCHITECTURE OF THE PROPOSED DETECTOR

Fig. 6 shows the architecture of the proposed successive interference cancellation two-user soft-detector. The baseband signal $y^{(k)}[n]$ is recovered with a single receiving antenna and radio-frequency front-end. The detector contains two branches, each detecting a different user. The upper branch performs first the soft-demodulation and detection of the user with the strongest received power. In the lower branch, the presumed signal contribution of the strongest user is subtracted from the received signal and the message of the weakest user is decoded. If only one user alone is detected by the synchronization stage, only the upper branch can be used, and the proposed detector falls back to the single-user soft-detector presented in Section II.

In the following derivations, we assume without loss of generality that $P_{\text{A}} > P_{\text{B}}$. The gateway is hence synchronized to user A. The received samples after synchronization are split into windows $y^{(k)}[n]$ of N samples, following the signal model from (6). The detector first dechirps each window of N samples, yielding the dechirped signal $\tilde{y}^{(k)}[n]$ whose expression is provided in (7). The operations used to detect the strongest user are strictly identical to those of the single-user detector presented in Section II. The soft-demodulator of (5) processes the dechirped signal $\tilde{y}^{(k)}[n]$ with $\sqrt{P} = \sqrt{P_{\text{A}}}$ and by considering the contribution of user B only as additional white noise. The LLRs $z_{\text{A}}^{\prime(k,m)}$ from the demodulator are then de-interleaved and fed to the SISO Hamming decoder from [40]. The output LLRs $v_{\text{A}}^{(m,k)}$

of the soft-decoder are subsequently re-interleaved and sent back to the soft-demodulator as apriori information. This iterative decoding of user A leverages the channel code to further overcome the interference of user B. Let N_I be the number of iterations carried out by the detector in the branch of the strongest user. We later show that two iterations are sufficient in practice and that selecting $N_I > 2$ does not significantly improve the decoding performance.

Upon execution of the N_I iterations in the upper branch, the interleaved LLRs $v_{\mathrm{A}}^{\prime(k,m)}$ after decoding are used by an interference-cancellation algorithm to estimate and subtract the contribution of user A from the dechirped signal $\tilde{y}^{(k)}[n]$. Let $\tilde{y}_{\mathrm{IC}}^{(k)}[n]$ be the interference-cancelled signal. Due to the STO τ, each window $\tilde{y}_{\mathrm{IC}}^{(k)}[n]$ contains two symbols of user B. The demodulation of the k-th symbol of user B hence requires specific matched filters that account for the STO τ on the windows $\tilde{y}_{\mathrm{IC}}^{(k)}[n]$ and $\tilde{y}_{\mathrm{IC}}^{(k+1)}[n]$ [41]. This asynchronous soft-demodulator outputs LLR values $z_{\mathrm{B}}^{\prime(k,m)}$ which are finally interleaved and used in a SISO Hamming decoder to produce estimates $\hat{b}_{\mathrm{B}}^{(p,k)}$ of the payload bits of user B. The decoding of user B is always done in a single iteration since it is not impaired by the interference of user A.

B. CANCELLATION OF THE STRONGEST USER

The proposed detector performs hard cancellation of the symbols of user A. To this end, the interleaved LLRs $v_{\mathrm{A}}^{\prime(k,m)}$ are mapped back to probabilities. The probability that user A transmitted the candidate symbol $\bar{s}$ in the k-th window is

$$p\left(s_{\mathrm{A}}^{(k)} = \bar{s} \middle| v_{\mathrm{A}}^{\prime(k,m)}\right) = \prod_{i=0}^{\mathrm{SF}-1} \frac{e^{g_i(\bar{s}) v_{\mathrm{A}}^{\prime(k,i)}}}{1 + e^{v_{\mathrm{A}}^{\prime(k,i)}}}. \tag{8}$$

The detector then selects the symbol $\hat{s}_{\mathrm{A}}^{(k)}$, which is the symbol that was the most likely to have been sent by user A

$$\hat{s}_{\mathrm{A}}^{(k)} = \arg\max_{\bar{s}} \; p\left(s_{\mathrm{A}}^{(k)} = \bar{s} \middle| v_{\mathrm{A}}^{\prime(k,m)}\right). \tag{9}$$

To subtract the estimated symbol $\hat{s}_{\mathrm{A}}^{(k)}$ from $\tilde{y}^{(k)}[n]$, the detector requires an estimate of its initial phase $\theta_{\mathrm{A}}^{(k)}$. We here re-use the estimator from [41], where $\theta_{\mathrm{A}}^{(k)}$ is estimated by retrieving the phase of the bin $\hat{s}_{\mathrm{A}}^{(k)}$ in the DFT $Y^{(k)}$, i.e., $\hat{\theta}_{\mathrm{A}}^{(k)} = \arctan(Y^{(k)}[\hat{s}_{\mathrm{A}}^{(k)}])$. The presumed contribution of user A is then cancelled from the dechirped signal $\tilde{y}^{(k)}[n]$

$$\tilde{y}_{\mathrm{IC}}^{(k)}[n] = \tilde{y}^{(k)}[n] - \sqrt{P_{\mathrm{A}}} e^{j\hat{\theta}_{\mathrm{A}}^{(k)}} e^{j2\pi \hat{s}_{\mathrm{A}}^{(k)} \frac{n}{N}}. \tag{10}$$

C. DEMODULATION OF THE WEAKEST USER

Since the gateway is not synchronized to user B, the demodulation of this user must take into account both the STO τ and the residual CFO Δf_c. Following the dechirped signal model of (7), as shown at the bottom of the page the symbol $\bar{s}_{\mathrm{B}}^{(k-1)}$ of user B is split over the two windows $\tilde{y}^{(k-1)}[n]$ and $\tilde{y}^{(k)}[n]$. Therefore, to detect $\bar{s}_{\mathrm{B}}^{(k-1)}$, the asynchronous soft-demodulator computes two partial DFTs $M_1^{(k-1)}$ and $M_2^{(k-1)}$ over the last $N - \lceil\tau\rceil$ samples of $\tilde{y}_{\mathrm{IC}}^{(k-1)}[n]$ and the first $\lceil\tau\rceil$ samples of $\tilde{y}_{\mathrm{IC}}^{(k)}[n]$, respectively

$$M_1^{(k-1)}\left[\bar{s}_{\mathrm{B}}^{(k-1)}\right] = \sum_{n=\lceil\tau\rceil}^{N-1} \tilde{y}_{\mathrm{IC}}^{(k-1)}[n] \cdot e^{-j2\pi \frac{(n-\lceil\tau\rceil)}{N}\left(\bar{s}_{\mathrm{B}}^{(k-1)} - \tau + N\frac{\Delta f_c}{f_s}\right)} e^{-j2\pi\tau u\left[n - n_{f,2}^{(k-1)}\right]}, \tag{11}$$

$$M_2^{(k-1)}\left[\bar{s}_{\mathrm{B}}^{(k-1)}\right] = \sum_{n=0}^{\lceil\tau\rceil-1} \tilde{y}_{\mathrm{IC}}^{(k)}[n] \cdot e^{-j2\pi \frac{(n+N-\lceil\tau\rceil)}{N}\left(\bar{s}_{\mathrm{B}}^{(k-1)} - \tau + N\frac{\Delta f_c}{f_s}\right)} e^{-j2\pi\tau u\left[n - n_{f,1}^{(k)}\right]}. \tag{12}$$

Both partial DFTs $M_1^{(k-1)}$ and $M_2^{(k-1)}$ correct the effects of the STO and the residual CFO on the dechirped signal.

If the symbols $s_{\mathrm{A}}^{(k)}$ have correctly been cancelled in $\tilde{y}_{\mathrm{IC}}^{(k)}[n]$, it can be shown that the likelihood that user B sent the candidate symbol $\bar{s}_{\mathrm{B}}^{(k-1)}$ is given by

$$\Lambda\left(\bar{s}_{\mathrm{B}}^{(k-1)} \middle| \tilde{y}_{\mathrm{IC}}^{(k)}[n]\right) = C' I_0\left(\frac{\sqrt{P_{\mathrm{B}}}}{\sigma^2} \left| Y_{\mathrm{B}}^{(k-1)}\left[\bar{s}_{\mathrm{B}}^{(k-1)}\right] \right|\right), \tag{13}$$

where $Y_{\mathrm{B}}^{(k-1)}[\bar{s}] = M_1^{(k-1)}[\bar{s}] + M_2^{(k-1)}[\bar{s}]$ is the summation of the two partial DFTs, and C' is a constant common to all symbols of user B [41]. Since the proposed detector does not iterate for the weakest user, the LLRs at the output of the soft-demodulator are evaluated as

$$z_{\mathrm{B}}^{\prime(k-1,m)} = \max_{\bar{s}:g_m(\bar{s})=1}\left[\log I_0\left(\frac{\sqrt{P_{\mathrm{B}}}}{\sigma^2}\left|Y_{\mathrm{B}}^{(k-1)}[\bar{s}]\right|\right)\right] - \max_{\bar{s}:g_m(\bar{s})=0}\left[\log I_0\left(\frac{\sqrt{P_{\mathrm{B}}}}{\sigma^2}\left|Y_{\mathrm{B}}^{(k-1)}[\bar{s}]\right|\right)\right]. \tag{14}$$

D. PERFORMANCE ANALYSIS

The performance of our two-user SIC detector is now analyzed for different parameters. In the following results, we always simulate a scenario with two interfering users using the same SF. The users have a received power difference $\Delta P = P_{\mathrm{A}} - P_{\mathrm{B}}$ of 1.5 dB. This choice of ΔP is motivated by the fact the spreading gain of the modulation increases by approximately 3 dB when the SF is incremented [43]. Therefore, in a network where the SFs of all users are optimally allocated, all nodes using the same SF should have at the gateway a difference of received powers ΔP of at most 3 dB.

$$\tilde{y}^{(k)}[n] = \begin{cases} \sqrt{P_{\mathrm{A}}} e^{j\theta_{\mathrm{A}}^{(k)}} e^{j2\pi\frac{n}{N}s_{\mathrm{A}}^{(k)}} + \sqrt{P_{\mathrm{B}}} e^{j\theta_{\mathrm{B}}^{(k-1)} + 2\pi\tau u\left[n - n_{f,1}^{(k)}\right]} e^{j2\pi\frac{(n+N-\tau)}{N}\left(s_{\mathrm{B}}^{(k-1)} - \tau + N\frac{\Delta f_c}{f_s}\right)} + \tilde{w}^{(k)}[n], & n \in \mathcal{N}_1 \\ \sqrt{P_{\mathrm{A}}} e^{j\theta_{\mathrm{A}}^{(k)}} e^{j2\pi\frac{n}{N}s_{\mathrm{A}}^{(k)}} + \sqrt{P_{\mathrm{B}}} e^{j\theta_{\mathrm{B}}^{(k)} + 2\pi\tau u\left[n - n_{f,2}^{(k)}\right]} e^{j2\pi\frac{(n-\tau)}{N}\left(s_{\mathrm{B}}^{(k)} - \tau + N\frac{\Delta f_c}{f_s}\right)} + \tilde{w}^{(k)}[n], & n \in \mathcal{N}_2 \end{cases} \tag{7}$$

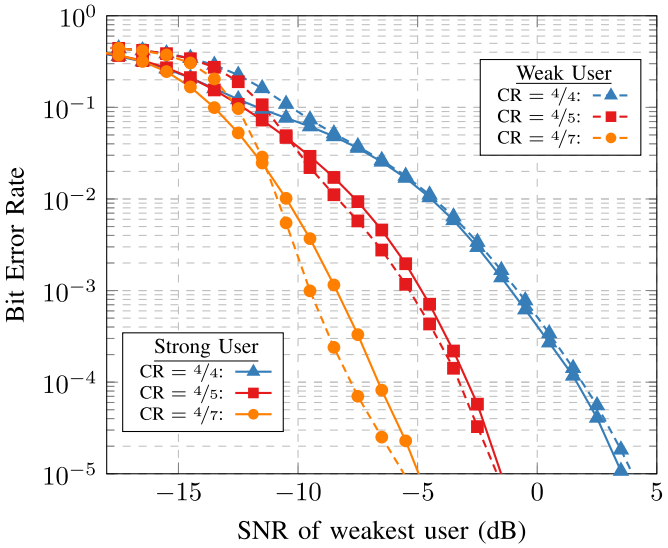

FIGURE 7. BERs of both users for different coding rates CR, with SF = 7, $\tau = 16.0$, $\Delta f_c = 0$ and $\Delta P = 1.5$ dB. For CR = 4/5 and 4/7, the strongest user is decoded with $N_I = 2$ iterations.

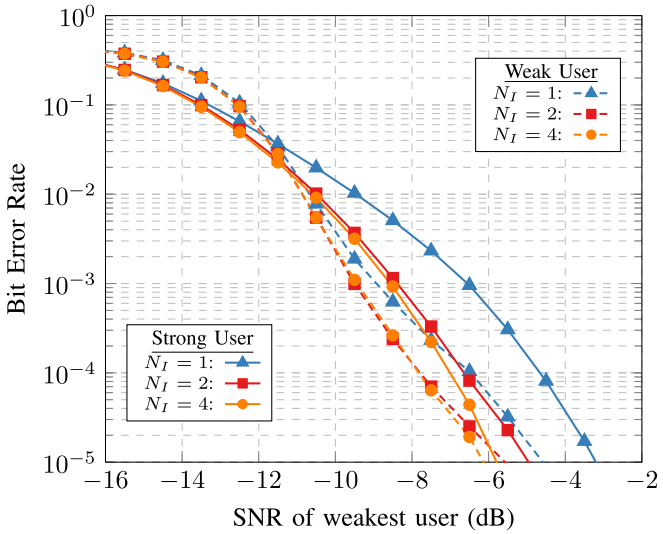

FIGURE 8. BERs of both users for different numbers of iterations in the decoding of the strongest user, with SF = 7, CR = 4/7, $\tau = 16.0$, $\Delta f_c = 0$ and $\Delta P = 1.5$ dB.

1) CODING RATE

We first study the impact of the coding rate on the decoding performance in a typical scenario with SF = 7. Fig. 7 shows the bit error rate (BER) of the strongest and weakest user, which are separated in time by a small STO $\tau = \frac{N}{8} = 16.0$. There is no residual CFO, i.e., $\Delta f_c = 0$. The strongest user is demodulated using $N_I = 2$ iterations.

In the absence of coding (CR = 4/4) and for a target BER of 10^{-4}, we observe that the strong and weak user need an SNR of 3.5 dB and 2 dB to be correctly demodulated, respectively. In a single-user scenario, this BER is attained for a much lower SNR of -7 dB [1]. When enabling the coding with CR = 4/5, the required SNRs to achieve the same BER are -1.5 dB and -3 dB for the strongest and weakest user, respectively, whereas in a single-user scenario, the corresponding SNR is at -8.5 dB. With CR = 4/7, the required SNRs even further decrease to -8 dB for both users. The required single-user SNR at this coding rate is -10 dB [1]. When comparing the required SNRs for the strongest user in the presence and the absence of a second user, we see that the gap reduces from 10.5 dB for CR = 4/4 to 2 dB for CR = 4/7. This important reduction indicates that the combination of the interleaving and the Hamming coding in the BICM scheme strongly helps a SIC soft-detector to demodulate the strongest user in the presence of same-SF interference.

2) NUMBER OF ITERATIONS

We now analyze the benefits of performing several iterations when demodulating the strongest user. For single-user BICM communications, it is well-known that Gray labeling offers the best first-pass performance, but yields no significant extra gain with iterative decoding [44]. These results have been confirmed in [1] for an iterative BICM LoRa single-user receiver. The authors show that for SF = 7, CR = 4/7 and a 10^{-4} BER, increasing the number of iterations from one to four only brings an SNR gain of 0.5 dB. We here show that in the case of our two-user SIC receiver, more significant SNR gains can be obtained.

Fig. 8 presents the BERs of both users for one, two and four iterations, with the same parameters as before and a coding rate of 4/7. In the present example, increasing N_I to two decreases the required SNR for the strongest user by 2 dB, and by 1.25 dB for the weakest user. Improving the demodulation of the strongest user also benefits the BER of the weakest user, as the contribution of the former is better cancelled before demodulating the latter. However, no further significant gains are observed for $N_I = 4$. We hence suggest limiting the number of iterations to two, in order to keep the complexity of the receiver as low as possible.

3) AVERAGING OVER STO AND CFO

The previous results have been obtained for specific values of STO τ and CFO Δf_c. However, it is important to note that the performance of a multi-user LoRa receiver strongly depends on the synchronization in time and frequency of the colliding users [11], [41], [45]. While the contribution of the strongest and synchronized user to the signal after dechirping $\tilde{y}^{(k)}[n]$ is always a Kronecker delta in the frequency domain, the spectral representation of the asynchronous user symbols is, depending on the STO and CFO, modified to a bell-shaped function that spreads across several DFT bins [11]. The more the signal of the asynchronous user is spread out, the higher is the probability of correctly decoding the synchronized user.

To better assess the performance of our proposed two-user detector in practical scenarios, Fig. 9 shows the averaged probability of correctly receiving the overlapping frames of two users for random values of τ and Δf_c, with $\Delta P = 1.5$ dB

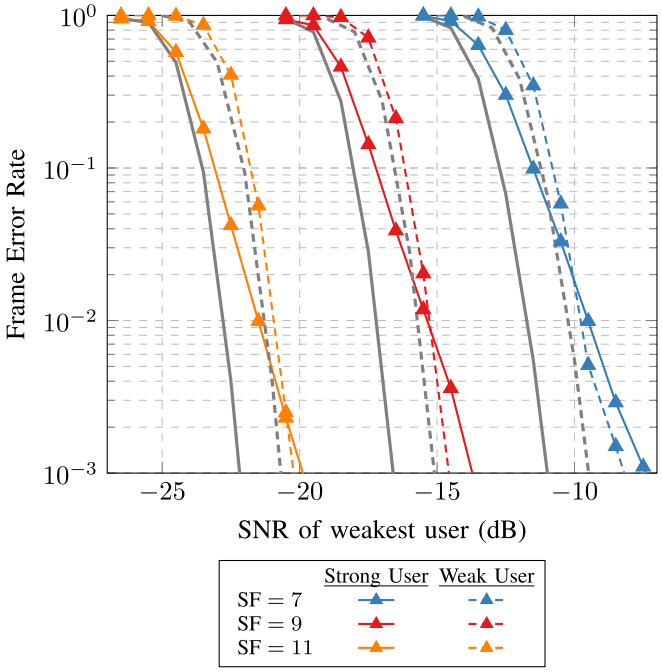

FIGURE 9. Averaged FERs of both users over random values of τ and Δf_c for different spreading factors, with $\Delta P = 1.5$ dB, CR = 4/7 and $N_I = 2$ iterations. For all spreading factors, the colliding frames have a length of 10 information bytes. The thick gray lines show the FER of the proposed receiver in the absence of a second user.

and CR = 4/7. The values of the STO τ and CFO Δf_c are uniformly distributed in the intervals $[0, N)$ and $[-\frac{f_s}{2N}, \frac{f_s}{2N}]$, respectively. The frame error rates (FERs) of the same detector in the presence of a single user at the same SNR levels (shown in gray) are also presented as baseline performance. For SF = 7 and a target FER of 10^{-2}, we observe that our SIC soft-receiver requires only 2 dB and 0.5 dB higher SNRs to demodulate the strongest and weakest user, respectively, compared to the corresponding single-user scenarios. At higher spreading factors, we also observe that our proposed detector fully benefits from the spreading gain of the modulation. These averaged FERs show that our proposed two-user receiver is capable of satisfactorily decoding the interfering users for all SFs, with only a small SNR penalty compared to the corresponding single-user scenarios.

IV. PERFORMANCE EVALUATION OF THE TWO-USER DETECTOR AT THE NETWORK-LEVEL

To better assess the benefits of the two-user soft-detector presented in Section III, this section presents a network-level performance evaluation using the discrete-event network simulator ns-3 [46]. To this end, we significantly extend the ns-3 LoRaWAN module from [7] to include models of (i) a single-user gateway with capture effect as modeled in [7] (ii) a more realistic parametric single-user soft-receiver PHY model and (iii) a detailed PHY model of our proposed two-user soft-detector. We first briefly explain how the network simulations are conducted within ns-3. We then describe the three studied LoRa gateway models, and we also explain the simulation parameters. On this basis, we finally analyze

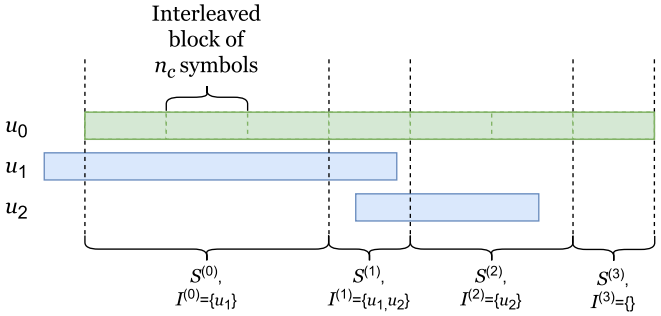

FIGURE 10. Illustration of subframe division for a frame of user u_0, colliding with the frames of two other same-SF interferers u_1 and u_2.

the performance of a LoRaWAN network using the different implemented gateway models to compare the single-user with the proposed two-user detector.

A. SIMULATION METHODOLOGY

We simulate a single LoRa cell, composed of one central gateway surrounded by end nodes. Both the gateway and the end nodes have models specifying their behaviour at the physical and MAC layers. We reuse all the models from [7], except the physical layer models that we substitute with more detailed and more accurate stochastic models. To evaluate the performance of the single- and two-user receivers, we perform Monte-Carlo (MC) simulations by computing for each packet the probability $p_{\text{err,frame}}$ that it is lost (i.e., the decoding led to one or more bit errors). The outcome of each frame (received or lost) is then decided accordingly at random using $p_{\text{err,frame}}$. To compute this probability, the frame under consideration is divided into N_S subframes $S^{(n)}$, with $n \in \{0, N_S - 1\}$. Let $I^{(n)}$ be the set of same-SF users that transmit a packet during the transmission of $S^{(n)}$. The division of the current frame into subframes is done such that each subframe has a set of interferers $I^{(n)}$ that is distinct from its neighbours $I^{(n-1)}$ and $I^{(n+1)}$, as illustrated in Fig. 10. The error probability $p_{\text{err}}^{(n)}$ of each subframe $S^{(n)}$ is evaluated using the PHY model of the gateway. Since the N_S error events of the subframes are independent, we can multiply them to obtain the overall frame error probability

$$p_{\text{err,frame}} = 1 - \prod_{n=0}^{N_S-1} \left(1 - p_{\text{err}}^{(n)}\right). \tag{15}$$

In our PHY models, we use look-up tables of FERs to rapidly access the probabilities $p_{\text{err}}^{(n)}$ which are obtained offline in PHY layer MATLAB Monte-Carlo simulations. To ensure the independence of the subframes, despite the coding and interleaver, these FERs can only be obtained for subframe lengths that are multiples of n_c symbols, i.e., the size of an interleaved block. We hence approximate the discretization of a frame into subframes $S^{(n)}$ to the closest interleaver boundaries.

Furthermore, due to the difference in nature between same-SF and inter-SF interference, these two kinds of collisions

need to be modeled differently. Same-SF interference is directly taken into account in all three considered PHY gateway models when we obtain the probabilities $p_{\text{err}}^{(n)}$ offline. To reduce the number of offline Monte-Carlo simulations, the inter-SF interference is modeled online within the network simulator by its impact on the signal-to-interference-plus-noise ratio (SINR). Since the dechirping sequence $x_0^*[n]$ used in the receivers is specific to each SF, the dechirped symbols of an interfering user using a different SF remain spread over the signal bandwidth. We therefore suggest to evaluate the SINR of each packet received at the gateway, and to use this ratio as SINR parameter in the error probabilities $p_{\text{err}}^{(n)}$. Let u be the user of interest, and $\bar{I}^{(n)}$ be the set of inter-SF interferers active during the transmission of the subframe $S^{(n)}$. We denote the received power of a user i at the gateway as P_i. To keep tractable models, we compute a single SINR value for each frame by selecting the highest interference level that is observed during its reception

$$\text{SINR} = \min_n \frac{P_u}{\sum\limits_{i \in \bar{I}^{(n)}} P_i + \sigma^2}. \tag{16}$$

The SINRs hence account for the inter-SF interference and the noise, but not the same-SF interference.

B. DESCRIPTION OF THE GATEWAY MODELS

We now describe the PHY layer models of the three evaluated receivers in more detail.

1) THRESHOLD-BASED SINGLE-USER RECEIVER

This model implements the behavior of a single-user LoRa gateway similarly to [7]. Two conditions on the SINR and on the level of same-SF interference need to be met for a subframe to be lost. The subframe is considered lost if the observed SINR is below a threshold $\mathcal{S}_{\text{SF}}$, which is defined as the required SINR to attain an uncoded FER of 0.1% for the SF used in the absence of both same-SF and inter-SF interference. In addition, a same-SF interferer is considered sufficiently strong to prevent the correct decoding of the user of interest if the received power of the interferer is less than 3 dB below that of the considered user [9]

$$p_{\text{err}}^{(n)} = \begin{cases} 1 \quad \text{if} \quad \begin{cases} 10\log\frac{P_u}{P_i} < 3 \text{ dB for any } i \in I^{(n)} \\ \text{or} \\ \text{SINR} < \mathcal{S}_{\text{SF}}, \end{cases} \\ 0 \quad \text{else.} \end{cases} \tag{17}$$

2) SINGLE-USER RECEIVER WITH SOFT-DECODING

Assuming a hard threshold for the capture effect as described above or in other publications [7], [9] is however pessimistic. In fact, in some cases, a packet can still be demodulated for lower differences in received power ΔP between two same-SF colliding nodes (same-SF SIR) [8]. To allow for a fair comparison between conventional single-user LoRa receivers and our proposed two-user receiver, we here seek to better model the performance of a single-user soft-detector in the presence of a single same-SF interferer. To this end, we evaluate in MATLAB the FERs of the single-user soft-detector presented in Section II, but with the two-user signal model of (6). Similarly to our proposed receiver, we assume that this single-user receiver is always capable of synchronizing itself to the strongest user, and that it performs two iterations of soft-demodulation and soft-decoding, but only for the strongest user. We compute, using MC simulations, a look-up table $\mathcal{L}_{1\text{U}}(\text{SF}, \text{CR}, \Delta P, \text{SINR}, L)$ of the FERs for given values of the SF, coding rate CR, same-SF SIR ΔP, SINR level and subframe length L in symbols. To reduce the dimensionality of this table, these FERs are computed by averaging over all possible values of the STO τ and residual CFO Δf_c, as explained in Section III.

Let $L^{(n)}$ be the length of the subframe under evaluation. We consider this subframe to be lost if any same-SF colliding frame has a greater received power, or if at least two other weaker same-SF colliding frames are present with same-SF SIRs that are lower than 3 dB. Otherwise, the probability of loss $p_{\text{err}}^{(n)}$ for this subframe is retrieved from the look-up table

$$p_{\text{err}}^{(n)} = \begin{cases} 1 \text{ if } \begin{cases} 10\log\frac{P_u}{P_i} < 0 \text{ dB for any } i \in I^{(n)} \\ \text{or} \\ 10\log\frac{P_u}{P_{i_1}} < 3 \text{ dB and } 10\log\frac{P_u}{P_{i_2}} < 3 \text{ dB}, \\ \text{for any } i_1 \in I^{(n)}, i_2 \in I^{(n)} \text{ s.t. } i_1 \neq i_2, \end{cases} \\ \mathcal{L}_{1\text{U}}\left(\text{SF}, \text{CR}, \frac{P_u}{P_i}, \text{SINR}, L^{(n)}\right) \text{ else.} \end{cases} \tag{18}$$

3) TWO-USER SIC RECEIVER WITH SOFT-DECODING

Similarly to the previous model, we also compute a look-up table $\mathcal{L}_{2\text{U}}$ of the FERs of our proposed two-user receiver using MATLAB MC simulations. Contrary to the single-user receiver, the table $\mathcal{L}_{2\text{U}}$ also contains FERs for values $10\log\frac{P_u}{P_i} < 0$ dB, since the two-user receiver also allows the demodulation of a weaker user. Nevertheless, in the presence of more than two concurrent same-SF users with sufficiently strong received powers, we assume that the subframe is lost. The corresponding subframe error rate lookup table for ns-3 corresponds to

$$p_{\text{err}}^{(n)} = \begin{cases} 1 \text{ if } \begin{cases} 10\log\frac{P_u}{P_{i_1}} < 3 \text{ dB and } 10\log\frac{P_u}{P_{i_2}} < 3 \text{ dB}, \\ \text{for any } i_1 \in I^{(n)}, i_2 \in I^{(n)} \text{ s.t. } i_1 \neq i_2, \end{cases} \\ \mathcal{L}_{2\text{U}}\left(\text{SF}, \text{CR}, \frac{P_u}{P_i}, \text{SINR}, L^{(n)}\right) \text{ else.} \end{cases} \tag{19}$$

C. SIMULATION PARAMETERS

We now discuss the system parameters used in our network-level simulations.

1) SPATIAL DISTRIBUTION OF THE NODES

The simulated network consists in a circular cell with a central gateway. The end nodes surround the gateway following a random uniform distribution. This distribution leads to a homogeneous node density in the cell.

TABLE 1. Outcome of the spreading factor allocation across the cell.

Spreading Factor	7	8	9	10	11	12
Radius [km]	3.32	3.99	4.80	5.76	6.93	8.32
Percentage of Nodes [%]	16	7	10	15	21	31

2) FRAME LENGTH

All frames are 25-bytes long, with 13 bytes corresponding to the LoRaWAN MAC header and 12 bytes for the application payload. This payload length respects the fair access policy of The Things Network [47].

3) FREQUENCY BANDS

To keep our simulations as focused as possible, we simulate in ns-3 only one frequency band. The throughput results obtained below can simply be multiplied by the number of frequency bands used in practice to obtain the overall network throughput.

4) CHANNEL PROPAGATION

A log-distance path loss model is used to evaluate the received power of each node at the gateway. According to [48], we fix the path loss exponent to 3.76 and the reference loss as 7.7dB at one meter. Those value are representative of an urban area, with a gateway located at a height of 15 meters. On top of the path loss model, we also add an SNR penalty of 3 dB to account for the RF noise figure and synchronization non-idealities.

5) SPREADING FACTOR ALLOCATION

We assume that all nodes follow a greedy behavior and select the lowest possible spreading factor to decrease their transmission time, and hence their energy consumption. The range of each SF is calculated based on the previously explained channel propagation model such that all nodes using this SF have an uncoded FER of at most 0.1% in the absence of any interference. This policy results in a central disc containing all nodes with SF 7, and non-overlapping annuli whose distances increase with the SFs. The range of each SF and the repartition of nodes per SF are listed in Table 1.

6) POWER ALLOCATION

Since the spreading gain of LoRa increases by 3 dB for each increment of the SF, the nodes inside the annuli have a received power difference among them of at most 3 dB. On the contrary, the nodes with SF 7, all located in the central disc, may have more significant received power differences between them depending on their location in the disk. To reduce the level of inter-SF interference and maintain decent SINRs for the most distant nodes in the cell, we reduce the power of SF 7 nodes in steps of 3 dB as they approach closer to the gateway while keeping the 0.1% FER constraint. Since LoRaWAN nodes can only vary their output power programmatically in the range 0 to 14 dBm, the nodes with the SFs from 8 to 12 always use the highest output power of 14 dBm, and the lowest transmit power for SF 7 nodes is 0 dBm. Fig. 11 summarizes the outcome of both the SF and power allocation in the simulated cell.

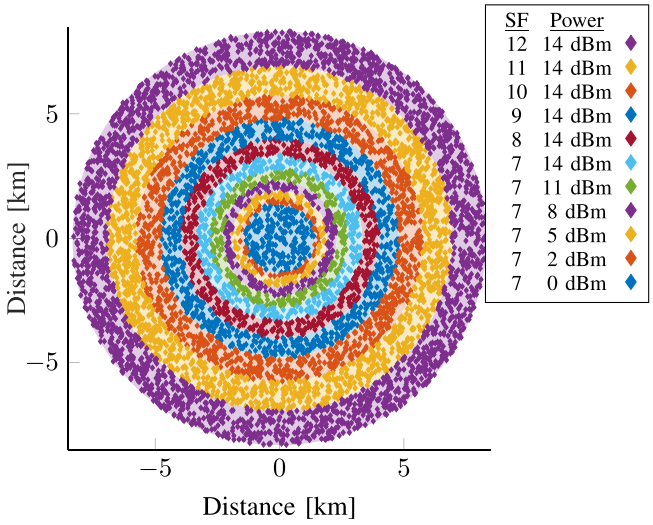

FIGURE 11. Power and spreading factor allocation within the cell.

D. RESULTS

We now evaluate and compare the system performance parameters with the three previously introduced models. We first study independently for each SF the gain in channel throughput of our proposed two-user detector compared to the two models of single-user receivers. We then perform an evaluation of the overall FER within the cell for an increasing node density, by taking into account all spreading factors.

1) THROUGHPUTS FOR A SINGLE SPREADING FACTOR

Fig. 12 presents the throughput attained for our proposed two-user detector and the two single-user models as a function of the offered load for the SFs 7 and 8, alongside the performance of single-user pure and slotted ALOHA, and two-user pure ALOHA schemes. To enable a better interpretation, and comparison of the results to the well studied baseline ALOHA performance, these first simulations use a single SF and ignore inter-SF interference.

We first study the throughput of the nodes with SF 8. We observe that the performance of the threshold-based single-user receiver model closely matches the throughput expectation of a pure ALOHA network. This result is expected as the only cause of packet losses are same-SF collisions, which are always destructive in the SF 8 annulus because all nodes have received powers in the same 3 dB range. On the contrary, thanks to the more precise modeling using look-up tables, we see that the real throughput of a single-user soft detector is significantly better compared to the pessimistic pure ALOHA model. Indeed, the single-user receiver is capable of sometimes recovering from same-SF collisions and successfully decode the frames of the strongest user, even when the power difference to the interferer is smaller than 3 dB. Its network performance, however,

remains below that of a pessimistic slotted ALOHA network. Regarding our proposed two-user soft-detector, we observe that its network throughput is only slightly below that of a the two-users pure ALOHA model. Since the two-user ALOHA model assumes an ideal detection of two colliding users, this result confirms that our detector is capable of decoding two colliding frames with a high reliability and that collisions between more than two users are rare.

The results observed in Fig. 12 hold for all the other SFs greater than 8. However, the throughput of SF 7 is a special case since the nodes using this SF are located in a disc, and not an annulus. Despite the power reduction scheme previously explained, these nodes benefit from a greater diversity of received powers. This wider power range increases the probability to benefit from the capture effect, therefore resolving some collisions without requiring any special treatment from the receiver. In our topology, this improved throughput concerns 16% of all nodes. The percentage of SF 7 nodes however increases when the cell size becomes smaller.

2) OVERALL THROUGHPUTS WITH ALL SPREADING FACTORS

We now analyze the overall frame error rate performance of a LoRaWAN network by also fully accounting for the inter-SF interference. Fig. 13 presents the global FER of a LoRaWAN network in which all nodes have a fixed duty cycle of 0.1% for an increasing density of users. We however note that modifying the transmission duty cycle parameter only result in a horizontal translation of the curves in Fig. 13. Furthermore, including for all users variable payload lengths between 1 and 25 bytes, instead of fixed payload lengths, leads to very similar results. The following analysis hence holds for all duty cycles and payload lengths.

In the following, we always target a FER of 1%. We first compare the two single-user models. We observe that the threshold-based model with capture is severely pessimistic, as the single-user soft-detector is actually capable of serving two times ($2\times$) more users thanks to its ability to sometimes recover the strongest one of two colliding users, even without coding. Also, the impact of the coding rate is not visible at all in the threshold-based model, as it solely uses the SINR of a frame to determine if it is correctly received. Conversely, the single-user soft-detector benefits from a decrease of the coding rate. However, at the network-level, the dominating error events remain the losses of the weakest users packets, and the benefits of the soft-decoding of the strongest user are hence marginal.

We finally evaluate the benefits of our proposed two-user SIC soft-detector at the network-level, compared to the single-user soft-detector. For a coding rate of $4/5$, we observe an increase of the node density for the 1% target FER by a factor 3.3. This gain even increases to a factor 4.7 when switching to a coding rate $4/7$. Contrary to the single-user detector, the coding rate plays a more important role for the two user detector as the dominating error events are

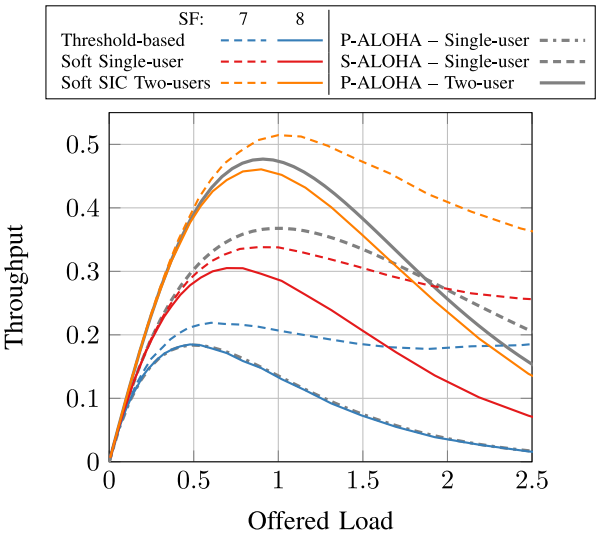

FIGURE 12. Throughput vs offered traffic for different receiver models and SFs with CR = 4/7, alongside the theoretical performance of pure ALOHA (P-ALOHA), slotted ALOHA (S-ALOHA), and pure two-user ALOHA networks.

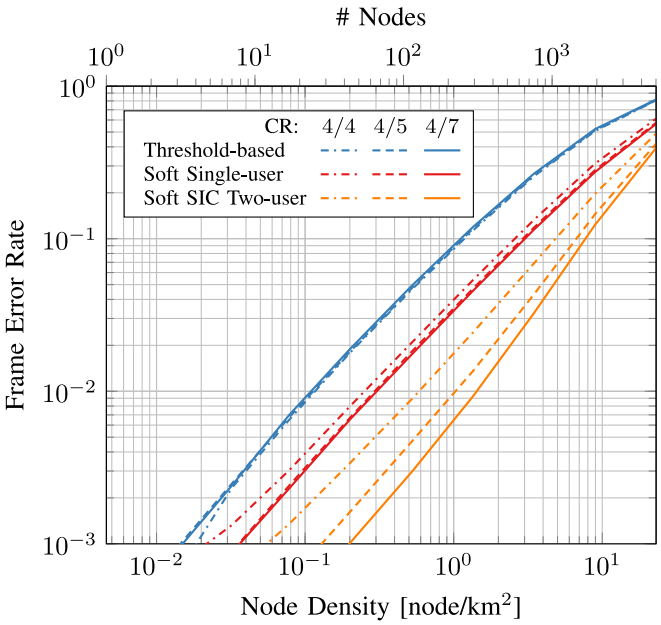

FIGURE 13. Frame error rate of a LoRaWAN network for different coding rates, with an uplink duty cycle of 0.1%.

not collisions among three users, which are very rare, but rather the incapacity of recovering the weakest user, which has a lower SINR. Specifically, in the simulated network, for a duty cycle of 0.1%, a target FER of 1% and CR = $4/7$, our two-user receiver enables a LoRaWAN gateway to serve 310 nodes, whereas a realistic model of a conventional single-user LoRaWAN gateway is only capable of serving 65 nodes.

V. CONCLUSION

Collisions between packets using the same spreading factor are the most important source of errors in dense LoRaWAN

networks. In this paper, we address this scalability limitation by designing a successive interference cancellation LoRa receiver capable of decoding two concurrent users with the same spreading factor. Our proposed two-user detector is the first to explicitly leverage the bit-interleaved coded modulation scheme of the LoRa physical layer with both a soft-demodulator and a soft-decoder to reach useful error rates in the low SNR regime that is characteristic for LoRa communications. Using Monte-Carlo simulations at the physical layer, we built accurate models of the frame error rates under same-SF interference of both a single-user LoRa soft-receiver and of our two-user soft-receiver for the network simulator ns-3. Network-level simulations indicate that our proposed two-user detector is capable of serving 4.7 times more nodes than a conventional single-user LoRa gateway, without requiring any modifications to the protocol.

SUPPLEMENTARY MATERIAL

The MATLAB implementation of the two-user soft-receiver, used to generate the results in Section III and the look-up tables of the PHY models in Section IV, is available on IEEE Xplore and on the Telecommunication Circuits Laboratory website [49].

REFERENCES

[1] T. Elshabrawy and J. Robert, "Evaluation of the BER performance of LoRa communication using BICM decoding," in *Proc. IEEE 9th Int. Conf. Consum. Electron. (ICCE-Berlin)*, 2019, pp. 162–167.

[2] A. Marquet, N. Montavont, and G. Z. Papadopoulos, "Investigating theoretical performance and demodulation techniques for LoRa," in *Proc. IEEE 20th Int. Symp. World Wireless Mobile Multimedia Netw. (WoWMoM)*, 2019, pp. 1–6.

[3] G. Callebaut, G. Ottoy, and L. Van der Perre, "Cross-layer framework and optimization for efficient use of the energy budget of IoT nodes," in *Proc. IEEE Wireless Commun. Netw. Conf. (WCNC)*, 2019, pp. 1–6.

[4] M. C. Bor, U. Roedig, T. Voigt, and J. M. Alonso, "Do LoRa low-power wide-area networks scale?" in *Proc. 19th ACM Int. Conf. Model. Anal. Simulat. Wireless Mobile Syst.*, 2016, pp. 59–67.

[5] O. Georgiou and U. Raza, "Low power wide area network analysis: Can LoRa scale?" *IEEE Wireless Commun. Lett.*, vol. 6, no. 2, pp. 162–165, Apr. 2017.

[6] D. Magrin, M. Centenaro, and L. Vangelista, "Performance evaluation of LoRa networks in a smart city scenario," in *Proc. IEEE Int. Conf. Commun. (ICC)*, 2017, pp. 1–7.

[7] D. Magrin, M. Capuzzo, and A. Zanella, "A thorough study of LoRaWAN performance under different parameter settings," *IEEE Internet Things J.*, vol. 7, no. 1, pp. 116–127, Jan. 2020.

[8] R. Fernandes, R. Oliveira, M. Luís, and S. Sargento, "On the real capacity of LoRa networks: The impact of non-destructive communications," *IEEE Commun. Lett.*, vol. 23, no. 12, pp. 2437–2441, Dec. 2019.

[9] D. Croce, M. Gucciardo, S. Mangione, G. Santaromita, and I. Tinnirello, "LoRa technology demystified: From link behavior to cell-level performance," *IEEE Trans. Wireless Commun.*, vol. 19, no. 2, pp. 822–834, Feb. 2020.

[10] J. Haxhibeqiri, F. Van den Abeele, I. Moerman, and J. Hoebeke, "LoRa scalability: A simulation model based on interference measurements," *Sensors*, vol. 17, no. 6, p. 1193, May 2017.

[11] O. Afisiadis, M. Cotting, A. Burg, and A. Balatsoukas-Stimming, "On the error rate of the LoRa modulation with interference," *IEEE Trans. Wireless Commun.*, vol. 19, no. 2, pp. 1292–1304, Feb. 2020.

[12] T.-H. To and A. Duda, "Simulation of LoRa in NS-3: Improving LoRa performance with CSMA," in *Proc. IEEE Int. Conf. Commun. (ICC)*, 2018, pp. 1–7.

[13] L. Beltramelli, A. Mahmood, P. Österberg, and M. Gidlund, "LoRa beyond ALOHA: An investigation of alternative random access protocols," *IEEE Trans. Ind. Informat.*, vol. 17, no. 5, pp. 3544–3554, May 2021.

[14] A. Gamage, J. C. Liando, C. Gu, R. Tan, and M. Li, "LMAC: Efficient carrier-sense multiple access for LoRa," in *Proc. 26th Annu. Int. Conf. Mobile Comput. Netw.*, Sep. 2020, pp. 1–13.

[15] T. Polonelli, D. Brunelli, A. Marzocchi, and L. Benini, "Slotted ALOHA on LoRaWAN—Design, analysis, and deployment," *Sensors*, vol. 19, no. 4, p. 838, Feb. 2019.

[16] B. Reynders, Q. Wang, P. Tuset-Peiro, X. Vilajosana, and S. Pollin, "Improving reliability and scalability of LoRaWANs through lightweight scheduling," *IEEE Internet Things J.*, vol. 5, no. 3, pp. 1830–1842, Jun. 2018.

[17] D. Zorbas, K. Abdelfadeel, P. Kotzanikolaou, and D. Pesch, "TS-LoRa: Time-slotted LoRaWAN for the Industrial Internet of Things," *Comput. Commun.*, vol. 153, pp. 1–10, Mar. 2020.

[18] J. Haxhibeqiri, I. Moerman, and J. Hoebeke, "Low overhead scheduling of LoRa transmissions for improved scalability," *IEEE Internet Things J.*, vol. 6, no. 2, pp. 3097–3109, Apr. 2019.

[19] R. Piyare, A. L. Murphy, M. Magno, and L. Benini, "On-demand LoRa: Asynchronous TDMA for energy efficient and low latency communication in IoT," *Sensors*, vol. 18, no. 11, p. 3718, Nov. 2018.

[20] S. Nagaraj, D. Truhachev, and C. Schlegel, "Analysis of a random channel access scheme with multi-packet reception," in *Proc. IEEE Global Telecommun. Conf.*, 2008, pp. 1–5.

[21] I. B. Arun and T. G. Venkatesh, "Order statistics based analysis of pure ALOHA in channels with multipacket reception," *IEEE Commun. Lett.*, vol. 17, no. 10, pp. 2012–2015, Oct. 2013.

[22] J. M. de Souza Sant'Ana, A. Hoeller, R. D. Souza, H. Alves, and S. Montejo-Sánchez, "LoRa performance analysis with superposed signal decoding," *IEEE Wireless Commun. Lett.*, vol. 9, no. 11, pp. 1865–1868, Nov. 2020.

[23] R. Eletreby, D. Zhang, S. Kumar, and O. Yağan, "Empowering low-power wide area networks in urban settings," in *Proc. Conf. ACM SIGCOMM*, Aug. 2017, pp. 309–321.

[24] B. Hu, Z. Yin, S. Wang, Z. Xu, and T. He, "SCLoRa: Leveraging multi-dimensionality in decoding collided LoRa transmissions," in *Proc. IEEE 28th Int. Conf. Netw. Protocols*, 2020, pp. 1–11.

[25] X. Xia, Y. Zheng, and T. Gu, "FTrack: Parallel decoding for LoRa transmissions," *IEEE/ACM Trans. Netw.*, vol. 28, no. 6, pp. 2573–2586, Dec. 2020.

[26] S. Tong, J. Wang, and Y. Liu, "Combating packet collisions using non-stationary signal scaling in LPWANs," in *Proc. 18th Int. Conf. Mobile Syst. Appl. Services*, Jun. 2020, pp. 234–246.

[27] M. O. Shahid, M. Philipose, K. Chintalapudi, S. Banerjee, and B. Krishnaswamy, "Concurrent interference cancellation: Decoding multi-packet collisions in LoRa," in *Proc. ACM SIGCOMM Conf.*, 2021, pp. 503–515.

[28] M. A. Ben Temim, G. Ferré, B. Laporte-Fauret, D. Dallet, B. Minger, and L. Fuché, "An enhanced receiver to decode superposed LoRa-like signals," *IEEE Internet Things J.*, vol. 7, no. 8, pp. 7419–7431, Aug. 2020.

[29] D. Garlisi, S. Mangione, F. Giuliano, D. Croce, G. Garbo, and I. Tinnirello, "Interference cancellation for LoRa gateways and impact on network capacity," *IEEE Access*, vol. 9, pp. 128133–128146, 2021.

[30] M. Xhonneux *et al.*, "A two-user successive interference cancellation LoRa receiver with soft-decoding," in *Proc. 55th Asilomar Conf. Signals Syst. Comput.*, to be published.

[31] M. Chiani and A. Elzanaty, "On the LoRa modulation for IoT: Waveform properties and spectral analysis," *IEEE Internet Things J.*, vol. 6, no. 5, pp. 8463–8470, Oct. 2019.

[32] R. Ghanaatian, O. Afisiadis, M. Cotting, and A. Burg, "LoRa digital receiver analysis and implementation," in *Proc. IEEE Int. Conf. Acoust. Speech Signal Process. (ICASSP)*, 2019, pp. 1498–1502.

[33] O. Afisiadis, A. Burg, and A. Balatsoukas-Stimming, "Coded LoRa frame error rate analysis," in *Proc. IEEE Int. Conf. Commun. (ICC)*, 2020, pp. 1–6.

[34] J. Tapparel, O. Afisiadis, P. Mayoraz, A. Balatsoukas-Stimming, and A. Burg, "An open-source LoRa physical layer prototype on GNU Radio," in *Proc. IEEE 21st Int. Workshop Signal Process. Adv. Wireless Commun. (SPAWC)*, 2020, pp. 1–5.

[35] M. C. Valenti and S. Cheng, "Iterative demodulation and decoding of turbo-coded M-ary noncoherent orthogonal modulation," *IEEE J. Sel. Areas Commun.*, vol. 23, no. 9, pp. 1739–1747, Sep. 2005.
[36] M. Xhonneux, O. Afisiadis, D. Bol, and J. Louveaux, "A low-complexity LoRa synchronization algorithm robust to sampling time offsets," *IEEE Internet Things J.*, early access, Jul. 29, 2021, doi: 10.1109/JIOT.2021.3101002.
[37] J. Proakis and M. Salehi, "Optimum receivers for AWGN channels," in *Digital Communications*. New York, NY, USA: McGraw-Hill, 2008, ch. 4, pp. 160–289.
[38] L. Vangelista, "Frequency shift chirp modulation: The LoRa modulation," *IEEE Signal Process. Lett.*, vol. 24, no. 12, pp. 1818–1821, Dec. 2017.
[39] M. Ivanov, C. Häger, F. Brännström, A. G. I. Amat, A. Alvarado, and E. Agrell, "On the information loss of the max-log approximation in BICM systems," *IEEE Trans. Inf. Theory*, vol. 62, no. 6, pp. 3011–3025, Jun. 2016.
[40] B. Müller, M. Holters, and U. Zölzer, "Low complexity soft-input soft-output hamming decoder," in *Proc. 50th FITCE Congr. ICT Bridging Ever Shifting Digital Divide*, 2011, pp. 1–5.
[41] M. Xhonneux, J. Tapparel, O. Afisiadis, A. Balatsoukas-Stimming, and A. Burg, "A maximum-likelihood-based multi-user LoRa receiver implemented in GNU radio," in *Proc. 54th Asilomar Conf. Signals Syst. Comput.*, 2020, pp. 1106–1111.
[42] O. Afisiadis, S. Li, J. Tapparel, A. Burg, and A. Balatsoukas-Stimming, "On the advantage of coherent LoRa detection in the presence of interference," *IEEE Internet Things J.*, vol. 8, no. 14, pp. 11581–11593, Jul. 2021.
[43] F. Van den Abeele, J. Haxhibeqiri, I. Moerman, and J. Hoebeke, "Scalability analysis of large-scale LoRaWAN networks in NS-3," *IEEE Internet Things J.*, vol. 4, no. 6, pp. 2186–2198, Dec. 2017.
[44] X. Li, A. Chindapol, and J. A. Ritcey, "Bit-interleaved coded modulation with iterative decoding and 8 PSK signaling," *IEEE Trans. Commun.*, vol. 50, no. 8, pp. 1250–1257, Aug. 2002.
[45] G. Ferré, B. Laporte-Fauret, and M. A. B. Temim, "A downlink non orthogonal multiple access for chirp spread spectrum communications," in *Proc. IEEE Latin-Amer. Conf. Commun. (LATINCOM)*, 2020, pp. 1–6.
[46] "NS-3 Network Simulator." NSNAM. 2021. [Online]. Available: https://www.nsnam.org/
[47] *Fair Use Policy Explained*, Things Netw., Amsterdam, The Netherlands, 2021. [Online]. Available: https://www.thethingsnetwork.org/forum/t/fair-use-policy-explained/1300
[48] "Radio frequency (RF) system scenarios (release 16)," 3GPP, Sophia Antipolis, France, Rep. 36.942, Jan. 2016.
[49] "A Multi-User LoRa Receiver Using Soft SIC Implemented in MATLAB." M. Xhonneux. 2021. [Online]. Available: https://www.epfl.ch/labs/tcl/resources-and-sw/matlab-soft-sic-lora-receiver/

JOACHIM TAPPAREL received the B.Sc. and M.Sc. degrees in electrical engineering from the École Polytechnique Fédérale de Lausanne, Lausanne, Switzerland, in 2018 and 2021, respectively, where he is currently pursuing the Ph.D. degree with the Telecommunications Circuits Laboratory.

His research interests include wireless communications for Internet-of-Things systems, digital signal processing for communications, and interference mitigation in communications.

MATHIEU XHONNEUX (Graduate Student Member, IEEE) received the M.Sc. degree in electrical engineering from the Université catholique de Louvain, Louvain-la-Neuve, Belgium, in 2018, where he is currently pursuing the Ph.D. degree in engineering science, under the supervision of Prof. J. Louveaux and Prof. D. Bol.

His current research interests include hardware/software co-design of signal processing systems and wireless communications for the Internet of Things.

DAVID BOL (Senior Member, IEEE) received the Ph.D. degree in engineering science from Université catholique de Louvain (UCLouvain), Louvain-la-Neuve, Belgium, in 2004 and 2008, respectively. In 2005, he was a visiting Ph.D student in advanced logic design with the CNM National Centre for Microelectronics, Sevilla, Spain. In 2009, he was a Postdoctoral Researcher with intoPIX, Louvain-la-Neuve, in low-power design for JPEG2000 image processing. In 2010, he was a Visiting Postdoctoral Researcher with UC Berkeley Laboratory for Manufacturing and Sustainability, Berkeley, CA, USA, in life-cycle assessment of the semiconductor environmental impact. He is currently an Assistant Professor with UCLouvain. In 2015, he participated to the creation of e-peas semiconductors, Louvain-la-Neuve. He leads the Electronic Circuits and Systems Group focused on ultra-low-power design of integrated circuits for environmental and biomedical IoT applications including computing, power management, sensing and wireless communications with a holistic focus on environmental sustainability. He is actively engaged in a social-ecological transition in the field of ICT research with a post-growth approach. He has authored or coauthored more than 150 technical papers and conference contributions and holds three delivered patents.

Dr. Bol (co-)received four Best Paper/Poster/Design Awards in IEEE conferences (ICCD 2008, SOI Conf. 2008, FTFC 2014, and ISCAS 2020) and was the Ph.D. supervisor of Charlotte Frenkel who received the 2021 Nokia Bell Scientific Award for her Ph.D. He served as an Editor for *Journal of Low Power Electronics and Applications* (MDPI), as a TPC Member of IEEE SubVt/S3S conference and currently serves as a reviewer for various journals and conferences such as IEEE JOURNAL OF SOLID-STATE CIRCUITS, IEEE TRANSACTIONS ON VERY LARGE SCALE INTEGRATION (VLSI) SYSTEMS, IEEE TRANSACTIONS ON CIRCUITS AND SYSTEMS—PART I: REGULAR PAPERS and IEEE TRANSACTIONS ON CIRCUITS AND SYSTEMS—PART II: EXPRESS BRIEFS. Since 2008, he presented several invited papers and keynote tutorials in international conferences including a forum presentation at IEEE ISSCC 2018.

JÉRÔME LOUVEAUX (Member, IEEE) received the electrical engineering degree and the Ph.D. degree from the Université catholique de Louvain (UCL), Louvain-la-Neuve, Belgium, in 1996 and 2000, respectively.

From 2000 to 2001, he was a Visiting Scholar with the Electrical Engineering Department, Stanford University, CA, USA. From 2004 to 2005, he was a Postdoctoral Researcher with the Delft University of Technology, Netherlands. Since 2006, he has been a Professor with the ICTEAM Institute, UCL. His research interests are in signal processing for digital communications, and in particular: multicarrier modulations, xDSL systems, resource allocation, synchronization and estimation. He was a co-recipient of the "Prix biennal Siemens 2000" for a contribution on filter-bank based multi-carrier transmission and the "Prix Scientifique Alcatel 2005" for a contribution in the field of powerline communications.

ANDREAS BURG (Senior Member, IEEE) was born in Munich, Germany, in 1975. He received the Dipl.-Ing. degree from the Swiss Federal Institute of Technology (ETH) Zurich, Zurich, Switzerland, in 2000, and the Dr.Sc.techn. degree from the Integrated Systems Laboratory, ETH Zurich, in 2006.

In 1998, he worked with Siemens Semiconductors, San Jose, CA, USA. During his doctoral studies, he worked with Bell Labs Wireless Research for a total of one year. From 2006 to 2007, he was a Postdoctoral Researcher with the Integrated Systems Laboratory and with the Communication Theory Group, ETH Zurich. In 2007, he Co-Founded Celestrius, an ETH-spinoff in the field of MIMO wireless communication, where he was responsible for the ASIC development as a Director for VLSI. In January 2009, he joined ETH Zurich as a SNF Assistant Professor and as the Head of the Signal Processing Circuits and Systems Group, Integrated Systems Laboratory. In January 2011, he joined the Ecole Polytechnique Federale de Lausanne where he is leading the Telecommunications Circuits Laboratory. He was promoted to an Tenure Associate Professor in June 2018.

Dr. Burg has served on the TPC of various conferences on signal processing, communications, and VLSI. He was a TPC Co-Chair for VLSI-SoC 2012, ESSCIRC 2016, and SiPS 2017. He was the General Chair of ISLPED 2019 and he served as an Editor for the IEEE TRANSACTION OF CIRCUITS AND SYSTEMS in 2013 and on the Editorial board of the *Microelectronics Journal* (Springer). He is currently an Editor of the *Journal on Signal Processing Systems* (Springer), *Journal on Low Power Electronics and its Applications* (MDPI), IEEE TRANSACTIONS ON VERY LARGE SCALE INTEGRATION (VLSI) SYSTEMS, and IEEE TRANSACTIONS ON SIGNAL PROCESSING. He is also a member of the EURASIP SAT SPCN and the IEEE CAS-VSATC.